

# On the delamination of thermal barrier coatings in a thermal gradient

J.W. Hutchinson<sup>a</sup>, A.G. Evans<sup>b,\*</sup>

<sup>a</sup>*Division of Engineering and Applied Science, Harvard University, Cambridge, MA 02138, USA*

<sup>b</sup>*Princeton Materials Institute, Princeton University, Princeton, NJ 08540, USA*

Received 2 April 2001; accepted in revised form 30 July 2001

## Abstract

Thermal barrier coating (TBC) systems are susceptible to delamination failures in the presence of a large thermal gradient. These failures, which occur within the TBC layer, are very different in character from those associated with the thermally grown oxide. Three possible causes of internal delamination are analyzed. In all cases, the thermomechanical properties of the TBC are allowed to vary because of sintering. (a) One mechanism relates to exfoliation of an internal separation in the TBC due to a through thickness heat flux. (b) Another is concerned with edge-related delamination within a thermal gradient. (c) The third is a consequence of sintering-induced stresses. The results of these analyses, when used in combination with available properties for the TBC, strongly suggest that the second mechanism (b) predominates in all reasonable scenarios. Consequences for the avoidance of this failure mode are discussed. © 2002 Elsevier Science B.V. All rights reserved.

**Keywords:** Thermal barrier coatings; Delamination; Thermal gradient; Sintering; Fracture toughness

## 1. Introduction

Multilayer thermal barrier systems are now commonly used in gas turbines. They comprise a single-crystal Ni alloy substrate, an intermediate Ni(Al) alloy layer (the bond coat) that acts as a barrier to oxidation, and an outer layer, typically yttria-stabilized zirconia, that provides the thermal insulation [1–10]. A thermally grown oxide (TGO), generally  $\alpha$ -Al<sub>2</sub>O<sub>3</sub>, forms between these two layers upon exposure to oxygen at high temperature. For high-performance systems, the TBC is manufactured by electron-beam physical vapor deposition (EB-PVD), imparting a columnar grain structure that provides strain tolerance [7–10]. Some failure modes originate in the vicinity of the interface, caused by the large residual compression that develops in the thin TGO layer upon thermal cycling [7–17]. Others occur internally, within the thermal barrier layer, especially in the presence of high heat flux (with an associated thermal gradient)

[18]. Mechanisms governing the former failure mode have been the subject of wide-ranging studies [6–8,10,13,19–22]. The latter mechanisms, which have not previously been examined in a systematic manner, will be addressed in the present article.

In the presence of a sufficient thermal gradient, cracks form and propagate on delamination planes in the TBC parallel to the interface, resulting in regions that spall away, leaving a thin layer of zirconia still attached to the substrate [18]. This failure mode does not arise either when the system is thermally cycled within a furnace (furnace cycle tests) or when tested in a burner rig. It is only activated in a high heat-flux environment. The challenge is to identify the origins of the stress, and hence the delamination energy release-rate. Two distinct possibilities are envisaged: both are defined, analyzed and compared.

1. An isolated crack parallel to the interface is envisaged, subject to a thermal gradient, that experiences an energy release rate and exfoliates (Fig. 1a). A similar crack is connected to either a free edge (Fig. 1b) or a crack through the thickness of the TBC.

\* Corresponding author. Tel.: +1-609-258-4762; fax: +1-609-258-1177.

E-mail address: anevans@princeton.edu (A.G. Evans).

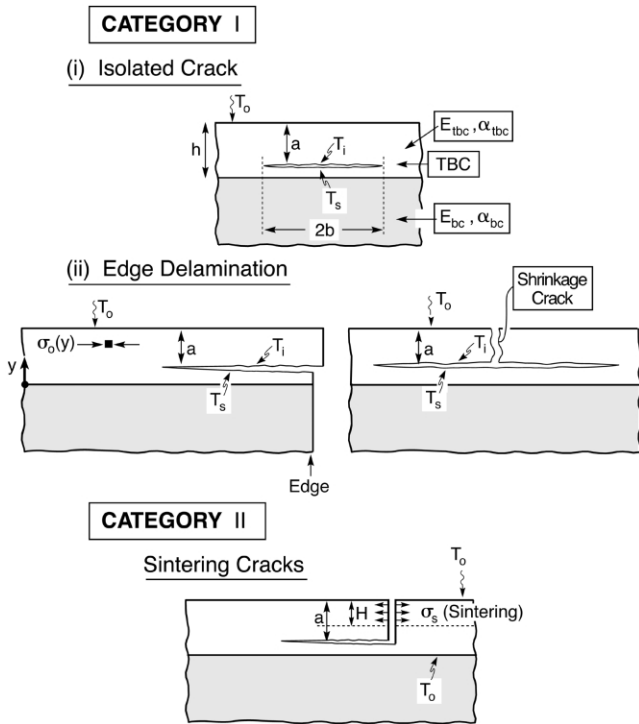


Fig. 1. Schematic of the three potential modes of delamination of a TBC in the presence of a thermal gradient.

2. A shrinkage crack caused by sintering of the top layer of the TBC [18], which may reorient into a delamination (Fig. 1c).

In all cases, the TBC is assumed to be stress-free at a reference temperature,  $T_{dep}$ , assumed to be equal to the deposition temperature (900–1000°C) [23]. Deviations from this temperature induce stresses because of the constraint of the superalloy substrate. Additional stresses are created by the presence of a thermal gradient. Both contributions to the stress are considered.

In the following, the energy release rate and the mode mixture are determined for each of the crack configurations and loadings. Comparing these with critical values for transverse cracking within the TBC predicts the most likely modes of delamination [18].

**2. Exfoliation**

*2.1. Isolated interface crack*

When a crack is isolated within the TBC, with no connection to the surface (Fig. 1a), the incidence of an energy release rate,  $G$ , is dictated by the conductivity of the crack. When the crack is conducting, such that the temperatures are the same on both crack faces,  $G$  is zero. The situation differs for insulated cracks that allow a temperature difference,  $\Delta T$ , to develop between the faces, as shown in Fig. 1a. The mechanics problem to

be addressed is shown in Fig. 2. Since the stresses caused by a thermal gradient (A) do not induce an energy release rate, the actual problem (B) can be solved by subtracting (A) from (B), resulting in the equivalent problem (C). In problem (C), the TBC away from the crack is at a uniform temperature ( $T=0$ ), while the crack faces experience a temperature differential,  $\Delta T=T_i-T_s$ . Then, if the coating has thickness,  $h$ , and the crack is in the TBC close to the interface ( $a \approx h$  in Fig. 2), the stresses  $\sigma_0$  in the TBC at a distance  $y$  above the crack are given by:

$$\sigma_0(y) = -\bar{E}_{tbc}\alpha_{tbc}\Delta T(1-y/h) \tag{1}$$

where  $\bar{E}_{tbc}$  is the modulus and  $\alpha_{tbc}$  is the thermal expansion coefficient for the TBC. The effect of this stress on  $G$  is ascertained by adopting the Eshelby strategy [24]. The section of coating above the crack is detached, leaving a gap. A moment,  $M_o$ , as well as an in-plane force,  $F_o$ , is imposed on the detached section to assure that it fits exactly within the gap. The moment and in-plane force (per unit length) are given by:

$$M_o = -(1/12)\bar{E}_{tbc}\alpha_{tbc}\Delta T h^2 \tag{2}$$

$$F_o = (1/2)\bar{E}_{tbc}\alpha_{tbc}\Delta T h$$

The detached section is ‘welded in place’ and then the agent applying  $M_o$  and  $F_o$  lets go. The final moment and force,  $M$  and  $F$ , are obtained by coupling the ends of the detached section to the remaining coating/

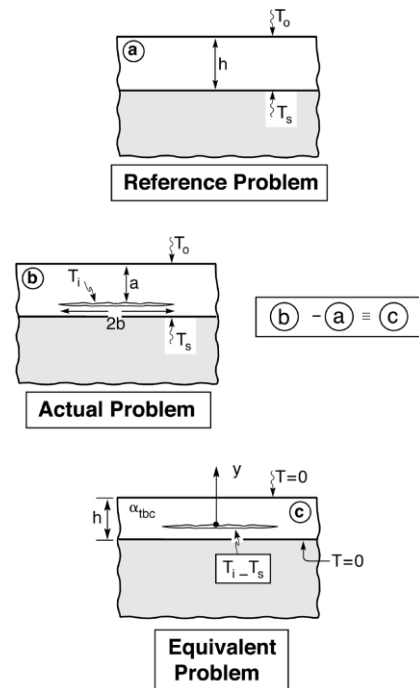


Fig. 2. The mechanics problem to be solved in order to assess the energy release rate for an isolated crack in the TBC subject to a heat flux.

substrate system by requiring continuity of moment, force, displacement and rotation. The displacement,  $u$ , and rotation,  $\theta$ , induced at the right-hand end in the remaining coating/substrate system are given by [26]:

$$u = a_{11}F/\bar{E}_{\text{tbc}} + a_{12}M/\bar{E}_{\text{tbc}}h \quad (3)$$

$$\theta = a_{12}F/\bar{E}_{\text{tbc}}h + a_{22}M\bar{E}_{\text{tbc}}h^2$$

The coefficients  $a_{ij}$  depend on the ratio of the crack size to coating thickness,  $b/h$ , and the two Dundurs' elastic mismatch parameters,  $\alpha_D = (\bar{E}_{\text{tbc}} - \bar{E}_{\text{substrate}})/(\bar{E}_{\text{tbc}} + \bar{E}_{\text{substrate}})$  and  $\beta_D$ . They have been tabulated by Yu and Hutchinson [26]. The second Dundurs' parameter,  $\beta_D$ , plays a minor role and it will be taken to be zero here. The corresponding displacement and rotation at the right end of the detached segment are given by:

$$u = (F_o - F)b/\bar{E}_{\text{tbc}}h \quad (4)$$

$$\theta = 12(M_o - M)b/\bar{E}_{\text{tbc}}h^3$$

Imposition of the continuity conditions for the two pieces using Eqs. (2)–(4) gives:

$$F = \frac{(b/h)(a_{22} + 12b/h)F_o - 12(b/h)a_{12}M_o/h}{\aleph} \quad (5)$$

$$M/h = \frac{12(b/h)(a_{11} + b/h)M_o/h - (b/h)a_{12}F_o}{\aleph}$$

$$\aleph = (a_{11} + b/h)(a_{22} + 12b/h) - a_{12}^2$$

The stress intensity factors induced by these displacements and rotations are expressed in terms of  $F$  and  $M$ . For  $\beta_D = 0$ , they can be written as [26]:

$$K_I^{\Delta T} = c_{21}F/\sqrt{h} + 2\sqrt{3}c_{22}M/h^{3/2} \quad (6)$$

$$K_{II}^{\Delta T} = c_{11}F/\sqrt{h} + 2\sqrt{3}c_{12}M/h^{3/2}$$

The coefficients  $c_{ij}$  are again functions of  $b/h$  and  $\alpha_D$ ; they have been tabulated by Yu and Hutchinson [26]. The energy release rate and mode mixture may be obtained from the stress intensity factors [25] as:

$$G^{\Delta T} = \frac{1}{2} \left( \frac{1}{\bar{E}_{\text{tbc}}} + \frac{1}{\bar{E}_{\text{substrate}}} \right) (K_I^{\Delta T 2} + K_{II}^{\Delta T 2})$$

$$\psi = \tan^{-1} \left( \frac{K_{II}^{\Delta T}}{K_I^{\Delta T}} \right) \quad (7a)$$

In the limit, when  $b/h \gg 1$ ,  $G$  approaches the limiting steady-state value:

$$G_{\text{ss}}^{\Delta T} = (1/2)F_o^2/\bar{E}_{\text{tbc}}h + 6M_o^2/\bar{E}_{\text{tbc}}h^3$$

$$\equiv \bar{E}_{\text{tbc}}(\alpha_{\text{tbc}}\Delta T)^2h/6 \quad (7b)$$

A plot of  $G^{\Delta T}/G_{\text{ss}}^{\Delta T}$  as a function of  $b/h$  is given in Fig. 3 for two values of  $\alpha_D$ : one corresponding to no elastic mismatch and the other to  $\bar{E}_{\text{tbc}}/\bar{E}_{\text{substrate}} = 1/3$ .

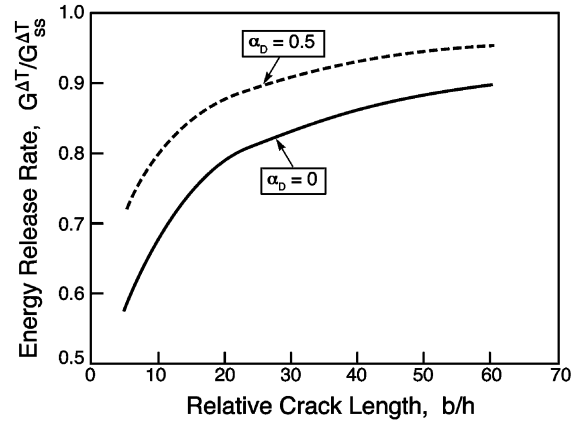


Fig. 3. The energy release rate as a function of crack length,  $2b$ , relative to coating thickness,  $h$ , for exfoliation of an isolated crack subject to a heat flux. The steady-state level is defined in the text.

The steady-state limit [Eq. (7b)] bounds the energy release rate from above and is only approached for fairly long cracks. The mode mixture associated with the entire range in Fig. 3 is predominately mode II with a small component of mode I [25]. The mode mixture has not been plotted.

Recall that for an isolated crack, there are no other contributions to  $G_{\text{ss}}^{\Delta T}$ : that is, even when stresses arise in the TBC because of thermal expansion misfit and thermal gradients, they do not induce an energy release rate [25]. The situation changes when the delamination is connected to a free edge (Fig. 1c) [18], as discussed next. Namely, the contribution in Eq. (6) still exists, but there is an extra contribution from the stresses in the TBC.

### 2.2. Edge delamination

When the TBC is at a higher temperature than the substrate and subject to a thermal gradient, two effects induce an energy release rate at an edge-connected delamination. Heating of the TBC above the stress-free temperature,  $T_{\text{dep}}$ , causes a thermal expansion misfit that places the TBC in residual compression. A superposed thermal gradient in the TBC induces a bending moment. The net effect is a stress distribution in the TBC given by:

$$\sigma(y) = \sigma_i(1 - y/h) + \sigma_o y/h \quad (8)$$

where  $\sigma_i$  is the stress at the TBC interface and  $\sigma_o$  the stress at the surface, with  $y$  being the distance from the interface. These stresses create a force and a moment (per unit length) in the absence of the delamination, given by:

$$F = (1/2)(\sigma_i + \sigma_o)h \quad (9)$$

$$M = -(1/12)(\sigma_i - \sigma_o)h^2$$

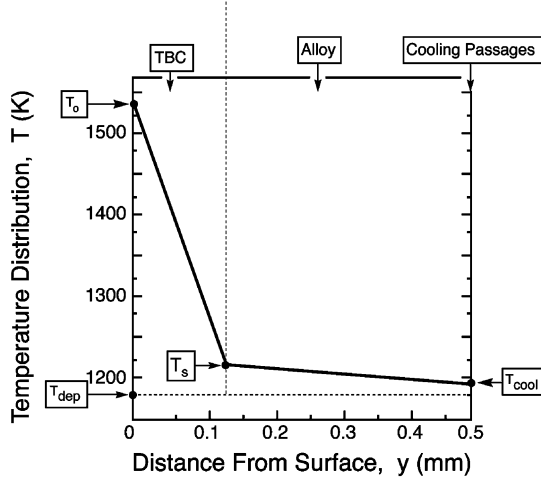


Fig. 4. A typical thermal profile within a TBC and substrate under operating conditions within a turbine [27].

When a delamination crack emerges from an edge along the interface, the force and moment are released, giving rise to an energy release rate which approaches from below the steady-state energy release rate [25]:

$$G_{ss}^{edge} = \frac{F^2}{2\bar{E}_{tbc}h} + \frac{6M^2}{\bar{E}_{tbc}h^3} \equiv \frac{\bar{\sigma}^2 h}{2\bar{E}_{tbc}} + \frac{\Delta\sigma^2 h}{24\bar{E}_{tbc}} \quad (10)$$

where  $\bar{\sigma} = (\sigma_i + \sigma_o)/2$  is the average stress in the TBC and  $\Delta\sigma = \sigma_o - \sigma_i$  is the stress difference between the top surface and the interface.

A prototypical steady-state temperature distribution for a thermal barrier system (Fig. 4) [27] is used to relate  $G_{ss}^{edge}$  to the thermal environment, with  $T_{dep}$  being the stress-free temperature,  $T_o$  the temperature at the TBC surface,  $T_i$  the temperature at the interface with the bond coat and  $T_{cool}$  the alloy temperature at the cooling channels. For this scenario, the temperature in the alloy is taken as  $\bar{T} = (T_i + T_{cool})/2$ , such that:

$$\Delta\sigma = \bar{E}_{tbc}\alpha_{tbc}(T_i - T_o) \quad (11)$$

$$\bar{\sigma} = 2\bar{E}_{tbc}\left\{\alpha_s(\bar{T} - T_{dep}) - \alpha_{tbc}[(T_o + T_i)/2 - T_{dep}]\right\}$$

Inspection of Eq. (10) and Eq. (11) indicates that for cases where  $T_{dep}$  is in the range 900–1000°C, and  $T_o$  is above 1200°C, the energy release is dominated by the  $\bar{\sigma}$  term in Eq. (10), which in turn is predominantly governed by the second term in Eq. (11), since the alloy temperature is near the deposition temperature. In other words, the dominant stress contribution is due to the elevation of the average temperature in the coating above the deposition temperature. Accordingly, the effective energy release rate becomes:

$$G_{ss}^{edge} \approx \left(\frac{\bar{E}_{tbc}h\alpha_{tbc}^2}{2}\right)[T_o + T_i - 2T_{dep}]^2 \quad (12)$$

This energy release is subject to strictly mode II (shear) loading, since  $\bar{\sigma}$  is a compression force [25].

### 3. Sintering cracks

When the top surface is at a sufficiently high temperature, the material begins to sinter, resulting in lateral shrinkage [18]. As the shrinkage occurs, in-plane tensile stresses are induced because of the constraint of the substrate. When this reaches the ‘sintering’ stress,  $\sigma_s$ , the lateral shrinkage stops. This stress is the product of the surface energy,  $\gamma_s$ , with curvature,  $\kappa$ , of those contacts between columns that experience neck growth and densification:  $\sigma_s = 2\gamma_s\kappa$  [28]. If it is large enough, the stress can cause ‘sintering’ cracks to form. If this stress develops over a depth,  $H$ , and a sintering crack forms through the thickness of the TBC [18], the crack could reorient into a delamination at depth  $a$ . Subject to this scenario, the energy release available for the delamination can be derived as follows.

The force and moment per unit length are:

$$F = \sigma_s H \quad (13)$$

$$M = (1/2)\sigma_s H(a - H)$$

where the moment is again taken at approximately the midplane of the coating. The steady-state energy release rate expression in Eq. (10) continues to hold, so that:

$$G_{ss}^{sinter} = \left(\frac{\sigma_s^2 H}{2\bar{E}_{tbc}}\right)\left[(H/a)\{1 + 3(1 - H/a)^2\}\right] \quad (14)$$

This result is plotted in Fig. 5.

The corresponding result for a crack of length  $a$  extending from the surface through the thickness and subject to a stress  $\sigma_s$  imposed over a segment of length  $H$  from the free surface ( $a > H$ ) is given by Tada et al. [29] for the case of no elastic mismatch:

$$G_{through} = \frac{4}{\pi} \left(\frac{\sigma_s^2 H}{\bar{E}_{tbc}}\right) \left(\frac{a}{H}\right) \times \left[ \left(1.30 - 0.18 \frac{H}{a}\right) \sin^{-1}\left(\frac{H}{a}\right) \right]^2 \quad (15)$$

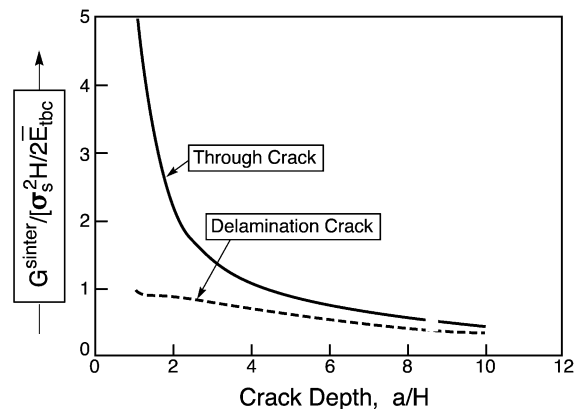


Fig. 5. The energy release rate for sintering-induced delamination as a function of crack depth.

Table 1  
Parameter range for analysis of energy release rates and delamination

TBC modulus, $E_{\text{tbc}}$ (GPa)	20–100
TBC thermal expansion coefficient, $\alpha_{\text{tbc}}$ (ppm °C <sup>-1</sup> )	13
Stress-free temperature, $T_{\text{dep}}$ (°C)	900–1000
Surface temperature of TBC, $T_o$ (°C)	1200–1300
Interface temperature, $T_2$ (°C)	1050
TBC thickness, $h$ (μm)	100
TBC toughness (J m <sup>-2</sup> )	
Mode I	5–20
Mode II	60–80

This result is also plotted in Fig. 5. The energy release rate of the mode I through-crack is always greater than that of the delamination crack at the same depth  $a$ , but the difference becomes small when the depth is four- or five-fold the sintering layer thickness. Since the delamination crack would normally extend along the trajectory with  $K_{\text{II}}=0$ , the preferred crack plane would be at  $a/H=3.86$ , such that the steady-state energy release rate becomes [25]:

$$G_{\text{ss}}^{\text{sinter}} = 0.343 \sigma_s^2 H / \bar{E}_{\text{tbc}} \quad (16)$$

Such a crack would be strictly mode I (opening).

## 4. Predominant mechanisms

### 4.1. Material properties

Insights into the phenomena most likely to cause delamination in the presence of a thermal gradient can be gained by comparing the energy release rates ascertained from Eqs. (7a), (7b), (12) and (16) for several prototypical scenarios and relating the absolute levels to the fracture toughness of the TBC. The parameter ranges indicated on Table 1 are used to conduct the estimates. The range in  $\bar{E}_{\text{tbc}}$  is used to explore the effect of sintering, which can elevate the high-temperature modulus from approximately 20 up to approximately 100 GPa [30,31]. The stress-free temperatures reflect the range used in commercial practice for EB-PVD coatings [23]. The surface temperature is taken to range from that used at present to temperatures expected for more aggressive designs, based on high-performance TBCs. The sintering stress is typical of that found for micron-sized necks in powder compacts [28]. The fracture toughness values have the following origins. The mode II toughness has been measured at ambient temperature by various impression tests: it is of order of  $\Gamma_{\text{II}} \approx 60$  J m<sup>-2</sup> [21,32,33a,33b]. The mode I toughness has not been measured for EB-PVD materials. For the present purposes, it is estimated, based on (i) similarity with plasma spray coatings [34] and (ii) typical ratios of mode I/mode II toughness for oxides [35]. This assessment infers a toughness of  $\Gamma_{\text{I}}=5\text{--}20$  J m<sup>-2</sup>, encompassing the mode I toughness for polycrystalline alumina

(the TGO), as well as that for the TGO/bond coat interface [8,21]. The through-thickness toughness is unknown, but should be much smaller than the transverse toughness (probably lower than 1 J m<sup>-2</sup>).

The sintering stress,  $\sigma_s = 2\gamma_s\kappa$ , with  $\gamma_s \approx 1$  J m<sup>-2</sup>, is entirely dependent on the curvature of the necks at the contacts between adjacent columns. Images of these necks [21,23] indicate typical values of  $\kappa \approx 2 \times 10^6$  m<sup>-1</sup> ( $\equiv 1$  μm neck diameters), such that  $\sigma_s \approx 4$  MPa. Slightly larger values (up to 10 MPa) are conceivable in some cases.

### 4.2. Through-cracks [18]

The only source of an energy release rate for cracks that might extend through the TBC is that related to the sintering stress [Eq. (15)]. The largest realistic values arise when there is a pre-existing crack,  $a \approx H$ , whereupon  $G_{\text{through}} \approx 0.1$  J m<sup>-2</sup>. While this is quite small, even for the low estimate of the toughness cited above, it must be large enough to cause through-cracks at temperatures where diffusional (creep) processes facilitate crack extension (similar to sintering cracks in other applications).

### 4.3. Delaminations [18]

The energy release rates for delamination due to the sintering stress [Eq. (16)] is approximately a factor of 10 less than that for the through-crack, and the toughness is much higher. These two factors *exclude delamination as a result of the sintering stress*. This would still be true if the sintering stress were appreciably larger (by an order of magnitude) than that cited in Table 1.

To address delamination of isolated cracks, the maximum achievable values in the thermal environment of the TBC are found by equating  $T_i$  to  $T_o$ , with the assumption that the TBC is transparent and radiation heats the top surface of the crack. Then  $G_{\text{ss}}^{\Delta T}$  ranges from 1 to 17 J m<sup>-2</sup>, with the largest value referring to a combination of the largest modulus (upon sintering of the TBC) and the greatest surface temperature. *Even the extreme value is lower than the mode II toughness relevant to this type of loading.*

Delamination from edges or through-cracks is much more probable, with the likelihood dependent on the incidence of TBC sintering [18]. The highest energy release rates arise whenever some sintering has occurred (such that  $\bar{E}_{\text{tbc}} \rightarrow 100$  GPa), and when the system is subject to a combination of the highest surface temperature with the lower deposition temperature. Then,  $G_{\text{ss}}^{\text{edge}}$  is over 200 J m<sup>-2</sup>, well above the mode II toughness (again the operative mode of loading), *whereupon delamination appears to be inevitable*. It is still just below the mode II toughness (approx. 50 J m<sup>-2</sup>) for a surface temperature of 1200°C and a deposition

temperature of 1000°C, conditions often encountered in advanced turbines. Delaminations can thus be envisaged as the TBC sinters and when surface temperatures reach extreme levels, either in the presence of a free edge or when a through-crack exists in the TBC (caused by sintering) [18].

In the absence of sintering ( $\bar{E}_{\text{tbc}} \approx 20$  GPa) these energy release rates decrease to approximately 40 and 10 J m<sup>-2</sup>, respectively, values either slightly or appreciably smaller than the mode II toughness, but similar to the mode I toughness. The implication is that delamination is unlikely, even at extremes of temperature, unless transverse loads are imposed that decrease the mode mixture (larger component of mode I).

In some instances, edge delamination may be exacerbated when the crack is insulating, such that the stress intensities from Eq. (6) superpose on those associated with Eq. (10). Conditions wherein this might occur remain to be addressed.

## 5. Conclusion

While three possible mechanisms of delamination in a thermal gradient have been analyzed, only one appears to be effective: namely, the edge delamination result expressed by Eq. (12). This result has several implications for conditions likely to activate this failure mode in preference to others (governed by the TGO). The most important parameters are the TBC modulus,  $\bar{E}_{\text{tbc}}$ , as well as the difference between the deposition and surface temperatures,  $T_{\text{dep}} - T_{\text{o}}$ . The delamination likelihood increases as either of these quantities increase. The modulus is primarily affected by sintering, governed in turn by both the material and the surface temperature. The temperature difference is associated with manufacturing conditions,  $T_{\text{dep}}$ , as well as the design of the turbine and the thermal conductivity of the TBC, which affect  $T_{\text{o}}$ .

## References

- [1] R.A. Miller, *J. Am. Ceram. Soc.* 67 (1984) 517.
- [2] J.T. DeMasi-Marcin, D.K. Gupta, *Surf. Coat. Technol.* 68/69 (1994).
- [3] R. Hillery (Ed.), *Coatings For High-Temperature Structural Application*, NRC Report, National Academy Press, 1996.
- [4] T.E. Strangman, *Thin Solid Films* 127 (1985) 93–105.
- [5] P.K. Wright, A.G. Evans, *Curr. Opin. Solid-State Mater. Sci.* 4 (1999) 255–265.
- [6] P.K. Wright, *Mater. Sci. Eng. A* 245 (1998) 191–200.
- [7] A.G. Evans, D.R. Mumm, J.W. Hutchinson, G.H. Meier, F.S. Pettit, *Prog. Mater. Sci.*, in press.
- [8] V. Sergo, D.R. Clarke, *J. Am. Ceram. Soc.* 81 (1998) 3237–3242.
- [9] J.R. Nicholls, *Mater. Sci. Forum* 935 (1997) 251–254.
- [10] S.R. Choi, J.W. Hutchinson, A.G. Evans, *Mech. Mater.* 31 (1999) 431–447.
- [11] D.M. Lipkin, D.R. Clarke, *Oxid. Met.* 45 (1996) 267–280.
- [12] V.K. Tolpygo, D.R. Clarke, *Oxid. Met.* 49 (1998) 187–211.
- [13] M.J. Stiger, N.M. Yanar, M.G. Topping, F.S. Pettit, G.H. Meier, *Z. Metall.* 90 (1999) 1069–1078.
- [14] R.J. Christensen, V.K. Tolpygo, D.R. Clarke, *Acta Mater.* 45 (1997) 1761–1766.
- [15] V.K. Tolpygo, D.R. Clarke, *Acta Mater.* 46 (1998) 5153–5166.
- [16] X-Y. Gong, D.R. Clarke, *Oxid. Met.* 50 (3/4) (1999) 355–376.
- [17] W.J. Quadackers, A.K. Tyagi, D. Clemens, R. Anton, L. Singheiser, in: J.M. Hampikian, N.B. Dahotre (Eds.), *Elevated Temperature Coatings: Science Technology*, TMS, Warrendale, PA, 1999, p. 119.
- [18] D. Zhu, R.A. Miller, B.A. Nagaraj, R.W. Bruce, *Surf. Coat. Technol.* 138 (2001) 1–8.
- [19] M. Gell, K. Vaidyanathan, B. Barber, J. Cheng, E. Jordan, *Met. Mater. Trans.* 30A (1999) 427.
- [20] A.G. Evans, J.W. Hutchinson, M.Y. He, *Acta Mater.* 47 (1999) 1513–1522.
- [21] D.R. Mumm, A.G. Evans, *Acta Mater.* 48 (2000) 1815–1827.
- [22] C. Mennicke, D.R. Mumm, D.R. Clarke, *Z. Metall.* 90 (1999) 1079–1085.
- [23] A. Mariochocchi, A. Bartz, D. Wortman, *Thermal Barrier Coating Workshop*, NASA CP 3312, 1995, p. 79.
- [24] J.D. Eshelby, *Proc. R. Soc. A* 244 (1952) 87–112.
- [25] J.W. Hutchinson, Z. Suo, *Adv. Appl. Mech.* 29 (1992) 62–191.
- [26] H.-H. Yu, J.W. Hutchinson, *Int. J. Solids Struct.*, submitted.
- [27] R. Siegel, C.M. Spruckler, *Mater. Sci. Eng. A* 245 (1998) 150–159.
- [28] W.D. Kingery, H.K. Bowen, D.R. Uhlmann, *Introduction to Ceramics*, Wiley and Sons, New York, 1976.
- [29] H. Tada, P.C. Paris, G.R. Irwin, *The Stress Analysis of Cracks Handbook*, 3rd, ASME Press, New York, 2000.
- [30] C.A. Johnson, J.A. Ruud, R. Bruce, D. Wortman, *Surf. Coat. Technol.* 108/109 (1998) 80.
- [31] S.R. Choi, D. Zhu, R.A. Miller, *Ceram. Eng. Sci.* 19 (1998) 293–301.
- [32] Y.C. Tsui, T.W. Clyne, in: C.C. Berndt (Ed.), *Thermal Spray Practical Solutions for Engineering Problems*, ASM International, 1996, p. 275.
- [33a] A. Vasinonta, J.L. Beuth, *Eng. Fracture Mech.*, in press.
- [33b] R. Handoko, J.L. Beuth, G.H. Meier, F.S. Pettit, M.J. Stiger, *Proceedings of the Materials Division Symposium on Durable Surfaces*, ASME Orlando, November 2000, Trans Tech Publications, Switzerland, 2000.
- [34] G. Quian, T. Nakamura, C.C. Berndt, *Mech. Mater.* 27 (1998) 91–110.
- [35] A.G. Evans, J.W. Hutchinson, Y. Wei, *Acta Mater.* 47 (1999) 4093–4113.